AGU PUBLICATIONS

Geophysical Research Letters

RESEARCH LETTER
10.1002/2016GL069067

Key Points:
- Observations and models are used to investigate what causes decadal variability of the South Atlantic MOC (SAMOC)
- A strong correlation is found between SAMOC and the leading mode of the South Atlantic sea surface height (SSH) variability
- Stationary Rossby wave and associated wind-stress curl forced by the IPO drive the variability of the South Atlantic SSH and thus the SAMOC

Supporting Information:
- Supporting Information S1

Correspondence to:
H. Lopez,
hlopez@rsmas.miami.edu

Citation:
Lopez, H., S. Dong, S.-K. Lee, and E. Campos (2016), Remote influence of Interdecadal Pacific Oscillation on the South Atlantic meridional overturning circulation variability, *Geophys. Res. Lett.*, *43*, 8250–8258, doi:10.1002/2016GL069067.

Received 11 APR 2016
Accepted 27 JUL 2016
Accepted article online 29 JUL 2016
Published online 14 AUG 2016

Remote influence of Interdecadal Pacific Oscillation on the South Atlantic meridional overturning circulation variability

Hosmay Lopez[1,2], Shenfu Dong[2], Sang-Ki Lee[2], and Edmo Campos[1,3]

[1]Cooperative Institute for Marine and Atmospheric Studies, University of Miami, Coral Gables, Florida, USA, [2]Atlantic Oceanographic and Meteorological Laboratory, NOAA, Miami, Florida, USA, [3]Oceanographic Institute of the University of São Paulo, São Paulo, Brazil

Abstract This study explores potential factors that may influence decadal variability of the South Atlantic meridional overturning circulation (SAMOC) by using observational data as well as surface-forced ocean model runs and a fully coupled climate model run. Here we show that SAMOC is strongly correlated with the leading mode of sea surface height (SSH) variability in the South Atlantic Ocean, which displays a meridional dipole between north and south of 20°S. A significant portion (~45%) of the South Atlantic SSH dipole variability is remotely modulated by the Interdecadal Pacific Oscillation (IPO). Further analysis shows that anomalous tropical Pacific convection associated with the IPO forces robust stationary Rossby wave patterns, modulating the wind stress curl over the South Atlantic Ocean. A positive (negative) phase IPO increases (decreases) the westerlies over the South Atlantic, which increases (decreases) the strength of the subtropical gyre in the South Atlantic and thus the SAMOC.

1. Introduction

The South Atlantic Ocean plays a key role in the global distribution of energy and is characterized by complex and unique ocean dynamic processes. For example, the Brazil-Malvinas Confluence [*Garzoli and Garraffo*, 1989; *Goni et al*., 2011] and the Agulhas leakage [*Gordon*, 1985; *Sloyan and Rintoul*, 2001] play critical roles in the exchange of water masses. These potentially modify the long-term response of the South Atlantic meridional overturning circulation (SAMOC) that could impact global atmospheric circulation, precipitation, and climate [*Sloyan and Rintoul*, 2001; *Reason*, 2001; *Suzuki et al*., 2004; *Haarsma et al*., 2005; *De Almeida et al*., 2007; *Garzoli and Matano*, 2011; *Lopez et al*., 2016].

For example, *Lopez et al.* [2016] showed that multidecadal variability of South Atlantic Ocean heat transport associated with the SAMOC plays a key role in modulating global atmospheric circulation via its influence on interhemispheric redistributions of atmospheric momentum, heat, and moisture. They found that decadal variations of South Atlantic heat transport could produce heat convergence/divergence in the tropical South Atlantic Ocean and thus modulate the strength of global monsoons with a time lag of about 20 years, suggesting that the SAMOC is a potential predictor of global monsoon variability.

Several studies have attempted to understand the possible mechanisms governing the strength of the SAMOC [*Delworth and Zeng*, 2008; *Wolfe and Cessi*, 2010]. *Biastoch et al.* [2009] and *Lee et al.* [2011] suggested a potential source of the anomalous SAMOC and meridional heat transport originating from the interocean transport from the Indian Ocean. *Yeager and Danabasoglu* [2014] found that most of the SAMOC variability is accounted for by changes in the Southern Hemispheric (SH) westerlies. However, other studies showed that the influence of SH wind stress onto the SAMOC depends on model representation of mesoscale eddies [*Farneti and Delworth*, 2010]. For instance, using an eddy-permitting model, *Gent and Danabasoglu* [2011] showed that the increase in the mean overturning circulation due to the acceleration of the SH westerlies is partially compensated by enhanced eddy transport. As such, there is currently little consensus about the underlying mechanism that governs SAMOC variability and how it might feedback into climate, mostly due to limited direct observations in the South Atlantic Ocean. Therefore, most of our current understanding of the SAMOC and its governing mechanism depend on the use of numerical models [e.g., *Stouffer et al*., 2006; *Smith and Gregory*, 2009].

Here we investigate how decadal variability of the SAMOC is forced. Given that El Niño–Southern Oscillation and associated atmospheric teleconnections explain a significant portion of wind-driven ocean circulation

variability in the South Atlantic [e.g., *Rodrigues et al*., 2015], we hypothesize that atmospheric teleconnections associated with diabatic heating from the Interdecadal Pacific Oscillation (IPO) could influence the South Atlantic wind stress field, thus modulate SAMOC. Our analysis will be based on existing observational products, surface-forced ocean model, and a fully coupled model run. The remaining of this paper is organized as follow: data sets and methodology are explained in section 2. Section 3 discusses the leading mode of sea surface height (SSH) variability in the South Atlantic and its relationship with SAMOC. Section 4 describes the Pacific-to-South Atlantic atmospheric teleconnections that could influence SAMOC variability. Summary and discussion are provided in section 5.

2. Data and Methodology

To assess SAMOC variability, we analyze observations, atmospheric reanalysis products, and model simulations. Observations used in this study include SSH from satellite altimetry for the period of 1993–2011 from the Archiving, Validation, and Interpretation of Satellite Oceanography [*Ducet et al*., 2000], sea surface temperature (SST) from the Extended Reconstructed Sea Surface Temperature version 3b for the period of 1900–2015, and atmospheric variables obtained from the NOAA-Cooperative Institute for Research in Environmental Sciences (CIRES) Twentieth Century Reanalysis [*Compo et al*., 2011] for the period of 1950–2012 and the ERA-20 Century Reanalysis [*Poli et al*., 2016] for the period of 1900–2010. An estimate of the SAMOC at 30°S is derived from *Dong et al.* [2015] (supporting information).

Observational records in the South Atlantic are short and sparse. Therefore, we use a combination of surface-forced and fully coupled models to investigate mechanisms of SAMOC variability. The surface-forced ocean model run is taken from the ocean-sea ice Parallel Ocean Program (POP2) model integrated using the NOAA-CIRES Twentieth Century Reanalysis [*Lee et al*., 2015]. We also forced the POP2 model with the ERA-Interim reanalysis from the European Centre for Medium-Range Weather Forecasts [*Dee et al*., 2011] as well as with the Modern-Era Retrospective Analysis for Research and Applications (MERRA) from NASA to validate our results. The NOAA-CIRES reanalysis forcing is from 1950 to 2012, whereas the ERA-Interim and MERRA forcing cover the period of 1979–2013. The coupled general circulation model used in this work is a 1000 year preindustrial simulation of the Community Earth System Model (CESM1) Large Ensemble Simulation [*Kay et al*., 2014]. The atmospheric component has 30 vertical levels with horizontal resolution of 1.25° in the zonal and 0.94° in the meridional direction. The ocean component has horizontal resolution of about 1°, with 60 vertical levels. The ocean and sea ice models are identical for the surface-forced and fully coupled runs.

3. Relationship Between SAMOC and Sea Surface Height

Principal component (PC) analysis was performed on the annual mean SSH from altimetry data and the surface-forced ocean model (POP2) over a rectangular box of the South Atlantic (60°W–20°E and 40°S–equator). The leading PC and associated spatial pattern are shown in Figure 1. Note that the SSH PC time series shows substantial low-frequency variability and is highly correlated with the SAMOC at 30°S, with correlation values of 0.85 and 0.71 for the observation and surface-forced ocean model, respectively. Both correlation values are significant at a 95% confidence level.

The spatial pattern associated with the leading PC, which is consistent between the observation and the surface-forced ocean model run, shows a meridional structure illustrating intensification/weakening of the South Atlantic subtropical gyre. This dominant mode of SSH variability is similar to the dominant mode of SST variability over the South Atlantic, which also shows a dipole-like pattern with centers of action over the tropical and subtropical South Atlantic [e.g., *Venegas et al*., 1997; *Sterl and Hazeleger*, 2003; *De Almeida et al*., 2007]. Several studies have investigated the physical mechanisms that drive the SST dipole structure in the South Atlantic [*Sterl and Hazeleger*, 2003; *Fauchereau et al*., 2003; *Morioka et al*., 2011]. These studies have concluded that the South Atlantic SST dipole could be driven by strengthening/weakening of the westerlies and southeasterlies, which in turn modulate the upper ocean mixing and surface turbulent heat fluxes.

To further explore the leading South Atlantic SSH mode of variability, we recalculate the SSH PC by using anomalies relative to the monthly mean data. The spatial pattern of monthly SSH PC is almost identical to that obtained from the annual mean field (Figure S1 in the supporting information). The surface-forced runs well reproduced the observed spatial and temporal evolution of the altimetry-derived SSH variability, independent of the atmospheric forcing used (Figure S1).

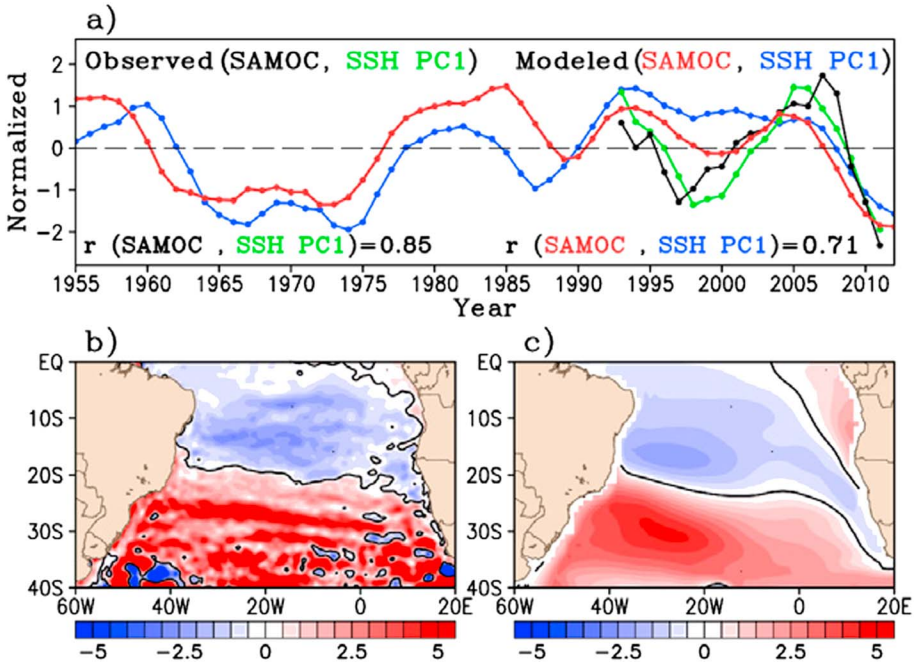

Figure 1. (a) Leading principal component PC of sea surface height (SSH) anomaly from the AVISO altimetry data set (green) and from the POP2 model (blue). Also shown is the SAMOC interannual anomaly estimate at 30°S from altimeter (black) and from the forced POP2 ocean model (red). The correlation between the SAMOC and the SSH PC is 0.85 for observations and 0.71 for the POP2 model. All time series were normalized to have unit variance. The spatial pattern of SSH associated with the leading PC (b) from observations and (c) from the POP2 model.

Figure 2 shows the regression of monthly SSH PC onto global SST anomaly for the observation, surface-forced ocean model run, and fully coupled model run. The global SST anomalies describe a meridional pattern in the South Atlantic from 60°S to the equator, similar to the spatial pattern of the leading SSH PC. There is large SST signal in the Pacific Ocean with positive anomalies over the central tropical Pacific near the North American coast and over the Southern Ocean south of 40°S between 180 and 60°W and negative anomalies over the western Pacific Ocean. This regressed global SST pattern is consistent between observation and models. The structure in the Pacific closely resembles that of the IPO [*Power et al*., 1999; *Folland et al*., 1999]. The remote influence of SST variability in the Pacific Ocean onto South Atlantic has been widely studied. For instance, *Rodrigues et al*. [2015] showed that the South Atlantic subtropical SST dipole (SASD) is sensitive to the location of SST anomalies in the tropical Pacific. Thus, a better understanding of how the SASD responds to IPO will contribute to more accurate climate predictions. Motivated by the relationship between the tropical Pacific SST anomalies and SASD, the remote relationship between the IPO and the leading SSH pattern in the South Atlantic is investigated in the next section.

4. IPO as Forcing of the South Atlantic MOC (SAMOC)

The IPO is a multidecadal SST mode of variability similar to El Niño–Southern Oscillation. It shows a symmetric structure about the equator. Otherwise, it is very similar to the Pacific Decadal Oscillation [*Mantua et al*., 1997]. The IPO is known to modulate the strength of the South Pacific convergence zone [*Folland et al*., 2002]. The reason we choose to assess the influence of the IPO onto the South Atlantic rather than the more traditional PDO is because the pattern in Figure 2 clearly resembles the IPO pattern. Also, the IPO is manifested throughout the Pacific Ocean and exhibits large interannual and decadal variabilities with considerable influence on tropical Pacific SST [*Folland et al*., 2002].

In order to verify the relationship between the South Atlantic SSH PC and the SAMOC with the IPO, we calculate an IPO index based on the difference between the SST anomaly averaged over the central equatorial Pacific (10°S–10°N, 170°E–90°W) and the average of the SST anomaly in the northwest (25°N–45°N,

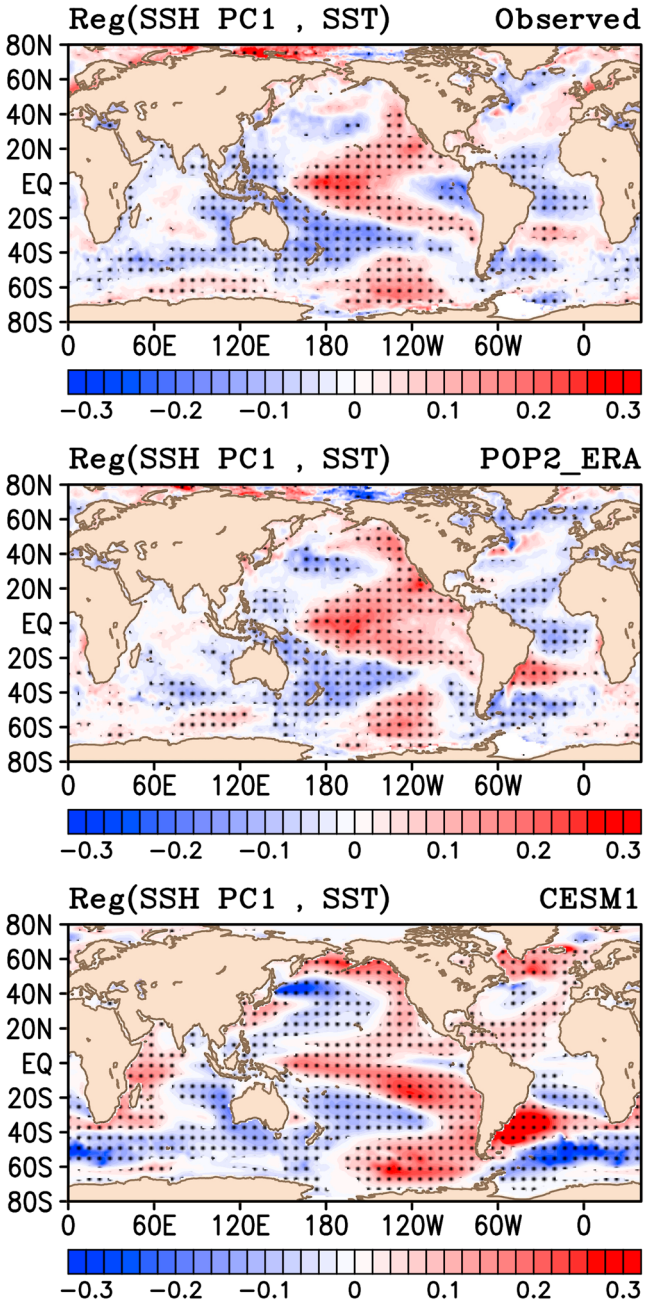

Figure 2. Regression of sea surface temperature (SST) onto the first principal component (PC) of sea surface height over the South Atlantic for (top) observed, (middle) ocean forced model, and (bottom) CESM1 model. The stipples indicate the statistical significance to a 95% confidence level from a Student's *t* test.

140°E–145°W) and southwest Pacific (50°S–15°S, 150°E–160°W) following *Henley et al.* [2015]. Figures 3a and 3b display the 11 year running mean IPO (black) and the leading South Atlantic SSH PC (green) derived from the forced ocean model and the CESM1, respectively. The IPO and the South Atlantic SSH PC are significantly correlated in both the forced ocean model (correlation of 0.43, significant at 90% percentile) and CESM1 model (correlation of 0.67, significant at 95% percentile). The leading SSH PC shows multidecadal variability with a statistical significant 10–15 year period (Figure S2), which is further supported by the similar spatial patterns of SST associated with the IPO (Figures 3d and 3e) and those obtained by regression of the South Atlantic SSH PC (Figure 2). The SST anomalies over the South Atlantic show a meridional dipole with warm (cold) anomalies north (south) of 40°S.

The global SST anomalies associated with the IPO and those associated with the South Atlantic SSH PC (Figure 2) are consistent in both the observations and the CESM1 model run, suggesting that the multicentury CESM1 run is a valid tool to assess the possible mechanism by which the IPO remotely forces the South Atlantic SSH and thus the SAMOC variability. The regression of monthly IPO index with 200 mb geopotential height (*Z*200) and rotational wind anomalies is shown in Figures 4a and 4b for CESM1 and ERA-20 Century Reanalysis, respectively. The *Z*200 associated with IPO clearly shows a stationary Rossby wave with positive height anomalies over the central tropical Pacific and cyclonic (anticyclonic) circulation south (north) of the equator, producing easterly flow at 200 mb along 45°S. This stationary wave pattern shows a negative (positive) *Z*200 anomaly south (north) of 40°S over the South Atlantic, which leads to westerly anomaly centered at about 40°S and easterly anomaly at 60°S as well as over the southern tip of Africa.

Upper level divergence forced by tropical heating associated with the IPO may initiate Rossby wave source, which may further force stationary Rossby waves to propagate to the midlatitudes. This relationship between upper level divergence and the remote circulation response is diagnosed by a Rossby wave source (equation (1)) defined by *Sardeshmukh and Hoskins* [1988].

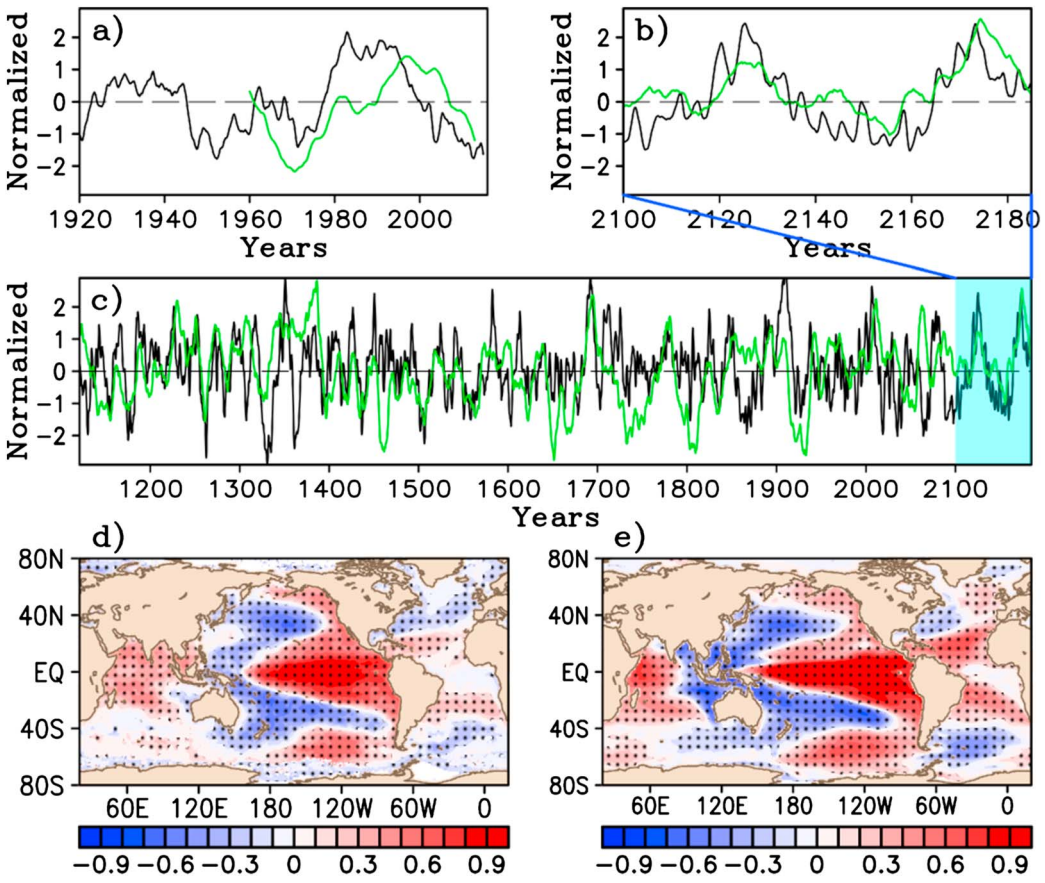

Figure 3. (a) Time series of Interdecadal Pacific Oscillation (IPO; black) and South Atlantic sea surface height PC (green) for the forced ocean model experiment. (b and c) The same as in Figure 3a but for the coupled CESM1 model run. The correlation between IPO and SSH PC is 0.43 (0.67) for the forced (coupled) model, respectively. The correlation for the coupled model is significant at a 95% confidence level, whereas that of the forced model is not significant due to reduced effective degrees of freedom. (d) Regression of observed IPO index onto observed SST. The stipples indicate the statistical significance to a 95% confidence level based on a Student's *t* test. (e) The same as in Figure 3d but for the CESM1 model.

$$\mathrm{RWS} = -\vec{V}_\chi \cdot \nabla(\zeta + f) - (\zeta + f)\nabla \cdot \vec{V}_\chi \tag{1}$$

Here ζ represents the relative vorticity and f is the Coriolis parameter. $\vec{V}_\chi$ is the divergent wind component at 200 mb and is obtained by solving the Poisson equation with 200 mb divergence as forcing following *Yu and Zwiers* [2007]. The Rossby wave source includes contribution from advection of absolute vorticity by the divergent wind and vortex stretching by the divergent wind.

We also investigated the stationary Rossby wave flux over the Southern Hemisphere (equation (2)) in order to assess stationary wave energy and teleconnection patterns associated with remote forcing (e.g., IPO forcing).

$$\rightarrow F = P \begin{pmatrix} \frac{1}{2a^2 \cos\varnothing}\left(\left(\frac{\partial\psi}{\partial\lambda}\right)^2 - \psi\frac{\partial^2\psi}{\partial\lambda^2}\right) \\ \frac{1}{2a^2}\left(\frac{\partial\psi}{\partial\lambda}\frac{\partial\psi}{\partial\varnothing} - \psi\frac{\partial^2\psi}{\partial\lambda\partial\varnothing}\right) \end{pmatrix} \tag{2}$$

This is a generalized version of the widely used Eliassen-Palm flux [*Andrews and McIntyre*, 1976] and can diagnose the propagation of stationary wave energy on a zonally asymmetric flow field. As in *Plumb* [1985], the horizontal component of the Rossby wave flux was computed in spherical coordinates. Here P is the pressure in hectopascal, a is the radius of the Earth in meters, $\varnothing$ represents the latitude, λ is the longitude, and ψ is the geostrophic stream function. The stream function is obtained by solving the Poisson equation with 200 mb relative vorticity as forcing.

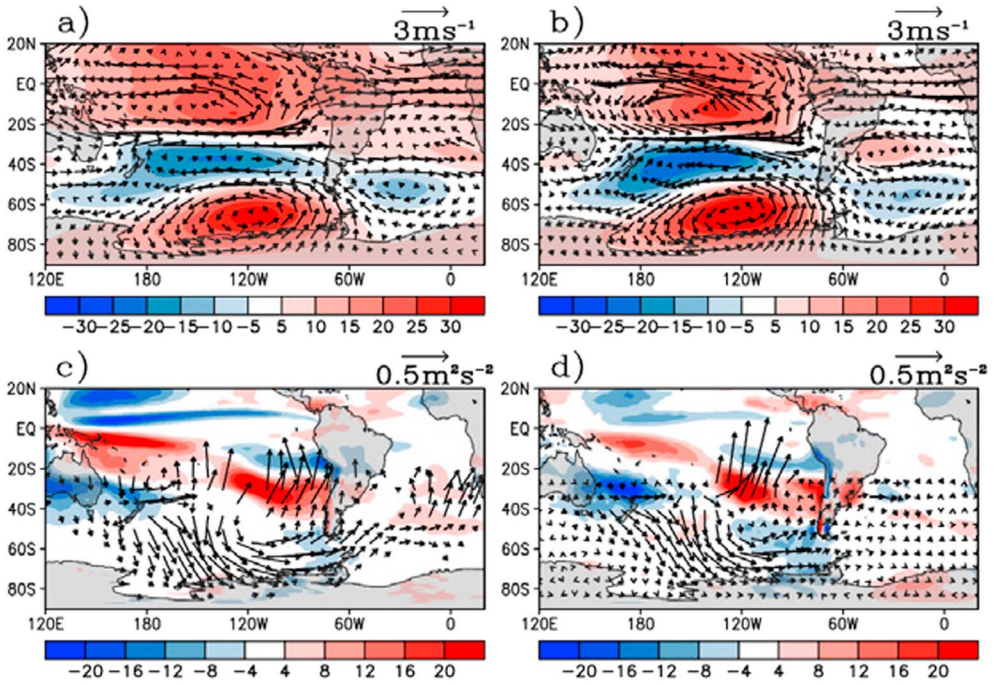

Figure 4. Regression of Interdecadal Pacific Oscillation (IPO) index with 200 mb geopotential height anomaly (color) and 200 mb rotational wind component (vector) for (a) CESM1 and (b) ERA-20 Century Reanalysis. The Rossby wave source (color with contour interval of 4.0×10^{-12} s^{-2}) and Rossby wave activity flux (vector) for (c) CESM1 and (d) ERA-20 Century Reanalysis. The positive (negative) Rossby wave source indicates the cyclonic (anticyclonic) source.

The 200 mb Rossby wave source (color) and stationary wave flux (vectors) are shown in Figures 4c and 4d for CESM1 and ERA-20 Century Reanalysis, respectively. Note that the major Rossby wave source regions associated with the IPO are in the western tropical Pacific and in the southeast subtropical Pacific near the South American coast. The former is dominated by meridional advection of absolute vorticity due to diabatic heating in the tropical Pacific (not shown). The latter is mostly due to vortex stretching by strong upper level divergence (not shown). Consistent with the Rossby wave flux, the stationary *Z*200 pattern originates from the Pacific Ocean as shown in Figures 4a and 4b. The Rossby wave response to IPO forcing has a considerable meridional component, which makes possible the incursion of Rossby wave activity toward the South Atlantic. This wave energy travels around the southern tip of South America converging in the South Atlantic Ocean. In general, the circulation patterns associated with IPO and its projection onto the South Atlantic Ocean sector are highly consistent between CESM1 and the ERA-20 Century Reanalysis, supporting our results.

The strongest Rossby wave flux signal associated with the IPO (Figures 4c and 4d) occurs over the anticyclonic circulation at around 120°W and 60°S. This anticyclone serves as a "blocking" pattern, which characterizes large-scale flow feature consisting of a dominant anticyclone poleward of a cyclone. In a similar way, the anomalous anticyclonic circulation could precondition the atmosphere to a state such that more blocking events occur in the eastern Pacific and Atlantic sector. Atmospheric blocking events lead to significant meridional shifts of the jet stream and storm track [*Scherrer et al.*, 2006]. This could potentially influence atmospheric forcing of the South Atlantic Ocean. To further assess the influence of the IPO onto atmospheric teleconnection pattern in the Pacific-South Atlantic sector, we look at atmospheric blocking frequency conditioned by the IPO state (Figure S3). A SH blocking index for each longitude is defined as in *Tibaldi et al.* [1994]. Here 3 day running average of 500 mb geopotential height is used to define blocking frequency. Then, a composite of blocking frequency is built based on the state of the IPO. Blocking events are significantly more common over the South Pacific and South Atlantic during the positive IPO phase (Figure S3). This is consistent with the stationary wave pattern shown in Figures 4a and 4b. The blocking events during a positive IPO occur around 55°S, causing a significant equatorial shift of the jet stream with anomalous positive zonal wind maxima around 40°S and negative anomalies around 60°S. This equatorward shift of the westerlies over the South Atlantic during positive IPO is depicted in Figure S4.

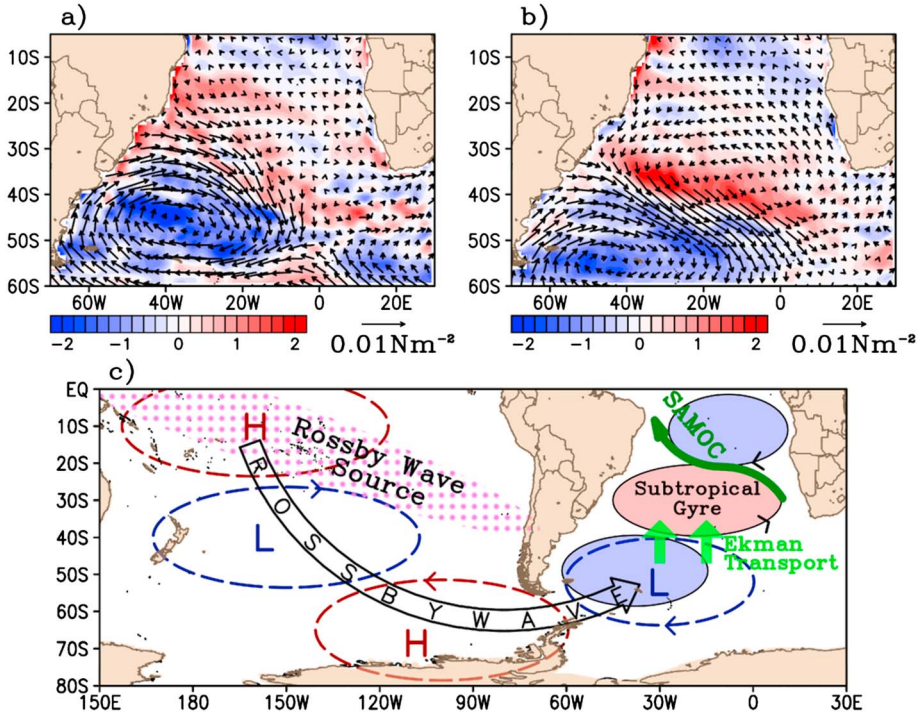

Figure 5. (a) Regression of SSH PC1 with surface wind stress (vector) and wind stress curl times Coriolis parameter (color) from altimetry data. (b) Same as in Figure 5a but for 20 Century Reanalysis. (c) Schematic diagram of the influence of the IPO on South Atlantic SSH and SAMOC variabilities. Heating anomaly in the atmosphere associated with the positive IPO generates Rossby wave source region extending from the tropical western Pacific toward South America (pink hatching). This generates a stationary wave pattern extending from the source region poleward around the southern tip of South America (labeled *H* and *L* for anticyclone and cyclone, respectively). This circulation produces anomalous westerlies in the South Atlantic between 30°S and 40°S, enhancing the northward Ekman transport, which in turn enhances the subtropical gyre circulation and northward SAMOC (dark green arrow).

We also tested the influence of other known teleconnection patterns that may influence South Atlantic SSH variability, namely, the Pacific South American (PSA1 and PSA2) patterns. These PSA modes are teleconnection patterns that exhibit significant variability ranging from subseasonal to decadal time scales [*Lau et al.*, 1994; *Sinclair et al.*, 1997; *Mo and Peagle*, 2001]. The PSA1 and PSA2 patterns are defined as the second and third empirical orthogonal function (EOF) modes of sea level pressure variability in the Southern Hemisphere. The first EOF mode is known as the Southern Annular Mode (SAM) [*Thompson and Wallace*, 2000]. The relationship between SAM and the South Atlantic SSH dipole is not explored here as they were shown to be independent [*Wang*, 2010].

Similarly to the IPO, the PSA1 and PSA2 patterns have strong seasonality in their variance (Figure S5), but their variances peak during austral winter as oppose to the IPO, which has the largest variance in austral summer. The difference in the seasonality of IPO and PSA1/PSA2 has great implication in their relative influence on the South Atlantic Ocean variability. The Rossby wave energy flux associated with the PSA patterns are more zonally oriented and confined to higher latitudes than those associated with the IPO (Figure S6). Indeed, the regression of wave energy flux with the South Atlantic SSH PC is very similar to that with the IPO but distinct from those with the PSA patterns.

The northward propagation of wave energy flux from the Drake Passage toward the South Atlantic associated with the IPO (Figures 4c and 4d) is possible due to a weaker subtropical jet during austral summer east of 150° E. In contrast, during austral winter when the PSA patterns are more active (Figure S5), the stronger subtropical jet acts as a waveguide, consequently inducing a zonally oriented (i.e., less South Atlantic incursion) wave flux. This result is consistent with *Berbery et al.* [1992]. They found that strong zonal flow (Figure S7) during austral winter produces negative meridional gradient of absolute vorticity, favoring a more robust zonal Rossby wave propagation.

5. Summary and Discussion

Using observations, atmospheric reanalysis products, and surface-forced and coupled models, we found that low-frequency variability of the SAMOC is tightly associated with the leading EOF of SSH in the South Atlantic Ocean. This EOF mode was described as a dipole in SSH with alternating sign north/south of 20°S and is strongly modulated by multidecadal variability in the Pacific Ocean, namely, the IPO.

The positive phase of the IPO is characterized by SST pattern that forces cyclonic and anticyclonic atmospheric Rossby waves extending from the tropical Pacific toward the South Atlantic. These Rossby waves have source regions that extend from the central Pacific southeastward toward the South American coast. This causes enhanced atmospheric blocking frequency west and east of the Drake Passage, consequently shifting the westerlies equatorward toward the South Atlantic. This in turn produces a northward Ekman transport, modulating the strength of the subtropical gyre in the South Atlantic (Figure 5c). This mechanism is verified by analyzing altimetry data as well as an ocean general circulation model forced with different atmospheric reanalysis data and a fully coupled model. The SSH dipole is associated with positive (negative) wind stress curl north (south) of 40°S due to northward shift of the westerlies over the Atlantic (Figures 5a and 5b).

This mechanism suggests that central Pacific SST anomalies associated with the IPO generate atmospheric Rossby waves to the Southern Hemisphere. Rossby wave generation associated with the IPO is not just confined to the tropical central Pacific; significant wave source is also present over the South Pacific convergence zone. The meridional propagation of wave energy flux into the South Atlantic is possible due to reduced subtropical jet in austral summer, consistent with the findings of *Rodrigues et al.* [2015], which argued that the South Atlantic Ocean is more readily influenced by remote forcing from the Pacific Ocean in the austral summer months.

Finally, this study brings some insight on the possibility of remote influence of Pacific multidecadal variability onto South Atlantic Ocean variability. Also, the results suggest that observed SSH could serve as proxy for SAMOC variability. These findings are important, given that factors influencing SAMOC variability are still not well understood. Future study will investigate the dependence of these results in an ocean eddy-resolving model run. We will also assess the influence of the South Atlantic SSH dipole and SAMOC on weather and climate over South America.

Acknowledgments

We acknowledge the anonymous reviewers as their comments have helped improve the manuscript. We would like to thanks Marlos Goes and Libby Johns (NOAA/AOML) for their comments. Data can be obtained upon request by contacting the corresponding author at hlopez@rsmas.miami.edu. This research was carried out under the auspices of the Cooperative Institute of Marine and Atmospheric Studies of the University of Miami and the National Oceanic and Atmospheric Administration (NOAA), cooperative agreement NA10OAR4320143. This work was supported by NOAA Atlantic Oceanographic and Meteorological Laboratory and funded by Climate Observations Division of the NOAA Climate Program Office. Dong is also partially supported by NOAA Climate Program Office and NASA grant NNH13AW33I E. Campos was partially supported by the Sao Paulo State Foundation (FAPESP, grant 2011/50552-4).

References

Andrews, D., and M. E. McIntyre (1976), Planetary waves in horizontal and vertical shear: The generalized Eliassen-Palm relation and the mean zonal acceleration, *J. Atmos. Sci.*, *33*(11), 2031–2048.

Berbery, E. H., J. Nogues-Paegle, and J. D. Horel (1992), Wave-like extratropical Southern Hemisphere teleconnections, *J. Atmos. Sci.*, *49*, 155–177.

Biastoch, A., C. W. Böning, F. U. Schwarzkopf, and J. Lutjeharms (2009), Increase in Agulhas leakage due to poleward shift of Southern Hemisphere westerlies, *Nature*, *462*(7272), 495–498.

Compo, G. P., et al. (2011), The Twentieth Century Reanalysis project, *Q. J. R. Meteorol. Soc.*, *137*, 1–28, doi:10.1002/qj.776.

De Almeida, R. A. F., P. Nobre, R. J. Haarsma, and E. J. D. Campos (2007), Negative ocean-atmosphere feedback in the South Atlantic convergence zone, *Geophys. Res. Lett.*, *34*, L18809, doi:10.1029/2007GL030401.

Dee, D. P., et al. (2011), The ERA-Interim reanalysis: Configuration and performance of the data assimilation system, *Q. J. R. Meteorol. Soc.*, *137*, 553–597, doi:10.1002/qj.828.

Delworth, T. L., and F. Zeng (2008), Simulated impact of altered Southern Hemisphere winds on the Atlantic overturning circulation, *Geophys. Res. Lett.*, *35*, L20708, doi:10.1029/2008GL035166.

Dong, S., G. Goni, and F. Bringas (2015), Temporal variability of the meridional overturning circulation in the South Atlantic between 20°S and 35°S, *Geophys. Res. Lett.*, *42*, 7655–7662, doi:10.1002/2015GL065603.

Ducet, N., P.-Y. Le Traon, and G. Reverdin (2000), Global high resolution mapping of ocean circulation from TOPEX/POSEIDON and ERS-1 and -2, *J. Geophys. Res.*, *105*, 19,477–19,498, doi:10.1029/2000JC900063.

Farneti, R., and T. L. Delworth (2010), The role of mesoscale eddies in the remote oceanic response to altered Southern Hemisphere winds, *J. Phys. Oceanogr.*, *40*, 2348–2354, doi:10.1175/2010JPO4480.1.

Fauchereau, N., S. Trzaska, Y. Richard, P. Roucou, and P. Camberlin (2003), Sea-surface temperature co-variability in the southern Atlantic and IndianOceans and its connections with atmospheric circulation in the SouthernHemisphere, *Int. J. Climatol.*, *23*, 663–677, doi:10.1002/joc.905.

Folland, C. K., D. E. Parker, A. Colman, and R. Washington (1999), Large scale modes of ocean surface temperature since the late nineteenth century, in *Beyond El Niño: Decadal and Interdecadal Climate Variability*, edited by A. Navarra, chap. 4, pp. 73–102, Springer, Berlin.

Folland, C. K., J. A. Renwick, M. J. Salinger, and A. B. Mullan (2002), Relative influences of the Interdecadal Pacific Oscillation and ENSO on the South Pacific convergence zone, *Geophys. Res. Lett.*, *29*(13), 1643, doi:10.1029/2001GL014201.

Garzoli, S. L., and R. Matano (2011), The South Atlantic and the Atlantic meridional overturning circulation, *Deep Sea Res. Part II*, *58*(17), 1837–1847.

Garzoli, S. L., and Z. Garraffo (1989), Transports, frontal motions and eddies at the Brazil-Malvinas Currents Confluence, *Deep Sea Res. Part A*, *36*(5), 681–703.
Gent, P. R., and G. Danabasoglu (2011), Response to increasing Southern Hemisphere winds in CCSM4, *J. Clim.*, *24*, 4992–4998, doi:10.1175/JCLI-D-10-05011.1.
Goni, G. J., F. Bringas, and P. N. Di Nezio (2011), Observed low frequency variability of the Brazil Current front, *J. Geophys. Res.*, *116*, C10037, doi:10.1029/2011JC007198.
Gordon, A. L. (1985), Indian-Atlantic transfer of thermocline water at the Agulhas Retroflection, *Science*, *227*(4690), 1030–1033.
Haarsma, R. J., E. J. D. Campos, W. Hazeleger, C. Severijns, A. R. Piola, and F. Molteni (2005), Dominant modes of variability in the South Atlantic: A study with a hierarchy of ocean–atmosphere models, *J. Clim.*, *18*, 1719–1735, doi:10.1175/JCLI3370.1.
Henley, B. J., J. Gergis, D. J. Karoly, S. B. Power, J. Kennedy, and C. K. Folland (2015), A tripole index for the Interdecadal Pacific Oscillation, *Clim. Dyn.*, *114*, doi:10.1007/s00382-015-2525-1.
Kay, J., C. Deser, A. Phillips, A. Mai, C. Hannay, G. Strand, J. Arblaster, S. Bates, G. Danabasoglu, and J. Edwards (2014), The Community Earth System Model (CESM) Large Ensemble Project: A community resource for studying climate change in the presence of internal climate variability, *Bull. Am. Meteorol. Soc.*, doi:10.1175/BAMS-D-13-00255.1.
Lau, W. K., P. J. Sheu, and I. S. Kang (1994), Multi-scale low frequency circulation modes in the global atmosphere, *J. Atmos. Sci.*, *51*, 2750–2753.
Lee, S. K., W. Park, E. van Sebille, M. O. Baringer, C. Wang, D. B. Enfield, S. G. Yeager, and B. P. Kirtman (2011), What caused the significant increase in Atlantic Ocean heat content since the mid-20th century?, *Geophys. Res. Lett.*, *38*, L17607, doi:10.1029/2011GL048856.
Lee, S.-K., W. Park, M. O. Baringer, A. L. Gordon, A. C. Clement, B. Huber, and Y. Liu (2015), Pacific origin of the abrupt increase in Indian Ocean heat content during the warming hiatus, *Nat. Geosci.*, *8*, 445–449.
Lopez, H., S. Dong, S. -K. Lee, and G. Goni (2016), Decadal modulations of interhemispheric global atmospheric circulations and monsoons by the South Atlantic meridional overturning circulation, *J. Clim.*, *29*, 1831–1851.
Mantua, N. J., S. R. Hare, Y. Zhang, J. M. Wallace, and R. C. Francis (1997), A Pacific interdecadal climate oscillation with impacts on salmon production, *Bull. Am. Meteorol. Soc.*, *78*, 1069–1079.
Mo, K., and J. N. Peagle (2001), The Pacific-South Atlantic modes and their downstream effects, *Int. J. Clim.*, *21*, 1211–1229.
Morioka, Y., T. Tozuka, and T. Yamagata (2011), On the growth and decay of the subtropical dipole mode in the South Atlantic, *J. Clim.*, *24*, 5538–5554, doi:10.1175/2011JCLI4010.1.
Plumb, R. A. (1985), On the three-dimensional propagation of stationary waves, *J. Atmos. Sci.*, *42*(3), 217–229.
Poli, P., et al. (2016), ERA-20C: An Atmospheric Reanalysis of the Twentieth Century, *J. Clim.*, *29*(11), 4083–4097.
Power, S., T. Casey, C. K. Folland, A. Colman, and V. Mehta (1999), Inter-decadal modulation of the impact of ENSO on Australia, *Clim. Dyn.*, *15*, 319–323.
Reason, C. J. C. (2001), Subtropical Indian Ocean SST dipole events and southern African rainfall, *Geophys. Res. Lett.*, *28*, 2225–2227, doi:10.1029/2000GL012735.
Rodrigues, R. R., E. J. D. Campos, and R. J. Haarsma (2015), The impact of ENSO on the South Atlantic subtropical dipole mode, *J. Clim.*, *28*, 2691–2705.
Sardeshmukh, P. D., and B. J. Hoskins (1988), The generation of global rotational flow by steady idealized tropical divergence, *J. Atmos. Sci.*, *45*, 1228–1251.
Scherrer, S. C., M. Croci-Maspoli, C. Schwierz, and C. Appenzeller (2006), Two-dimensional indices of atmospheric blocking and their statistical relationship with winter climate patterns in the Euro-Atlantic region, *Int. J. Clim.*, *26*(2), 233–250.
Sinclair, N. A., J. A. Renwick, and J. W. Kidson (1997), Low frequency variability of Southern Hemisphere sea level pressure and weather system activity, *Mon. Weather Rev.*, *125*, 2531–2543.
Sloyan, B. M., and S. R. Rintoul (2001), The southern ocean limb of the global deep overturning circulation, *J. Phys. Oceanogr.*, *31*(1), 143–173.
Smith, R. S., and J. M. Gregory (2009), A study of the sensitivity of ocean overturning circulation and climate to freshwater input in different regions of the North Atlantic, *Geophys. Res. Lett.*, *36*, L15701, doi:10.1029/2009GL038607.
Sterl, A., and W. Hazeleger (2003), Coupled variability and air–sea interaction in the South Atlantic Ocean, *Clim. Dyn.*, *21*, 559–571, doi:10.1007/s00382-003-0348-y.
Stouffer, R. J., J. Yin, J. Gregory, K. Dixon, M. Spelman, W. Hurlin, A. Weaver, M. Eby, G. Flato, and H. Hasumi (2006), Investigating the causes of the response of the thermohaline circulation to past and future climate changes, *J. Clim.*, *19*(8), 1365–1387.
Suzuki, R., S. K. Behera, S. Iizuka, and T. Yamagata (2004), Indian Ocean subtropical dipole simulated using a coupled general circulation model, *J. Geophys. Res.*, *109*, C09001, doi:10.1029/2003JC001974.
Thompson, D. W. J., and J. M. Wallace (2000), Annular modes in the extratropical circulation. Part I: Month-to-month variability, *J. Clim.*, *13*, 1000–1016.
Tibaldi, S., E. Tosi, A. Navarra, and L. Pedulli (1994), Northern and Southern Hemisphere seasonal variability of blocking frequency and predictability, *Mon. Weather Rev.*, *122*, 1971–2003.
Venegas, S. A., L. A. Mysak, and D. N. Straub (1997), Atmosphere–ocean coupled variability in the South Atlantic, *J. Clim.*, *10*, 2904–2920, doi:10.1175/1520-0442(1997)010,2904:AOCVIT.2.0.CO;2.
Wang, F. (2010), Subtropical dipole mode in the Southern Hemisphere: A global view, *Geophys. Res. Lett.*, *37*, L10702, doi:10.1029/2010GL042750.
Wilson, A. B., D. H. Bromwich, K. M. Hines, and S. H. Wang (2014), El Niño flavors and their simulated impacts on atmospheric circulation in the high-southern latitudes, *J. Clim.*, *27*, 8934–8955, doi:10.1175/JCLI-D-14-00296.1.
Wolfe, C. L., and P. Cessi (2010), What sets the strength of the middepth stratification and overturning circulation in eddying ocean models?, *J. Phys. Oceanogr.*, *40*, 1520–1538, doi:10.1175/2010JPO4393.1.
Yeager, S., and G. Danabasoglu (2014), The origins of late-twentieth-century variations in the large-scale North Atlantic circulation, *J. Clim.*, *27*, 3222–3247.
Yu, B., and F. W. Zwiers (2007), The impact of combined ENSO and PDO on the PNA climate: A 1, 000-year climate modeling study, *Clim. Dyn.*, *29*, 837–851.